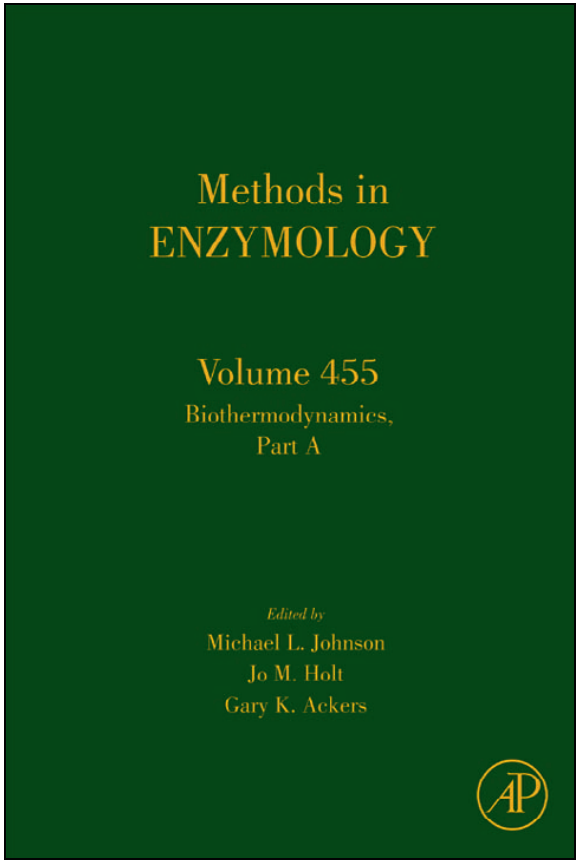

From: Gregory Benison and Elisar Barbar, NMR Analysis of Dynein Light Chain Dimerization and Interactions with Diverse Ligands.
In Michael L. Johnson, Jo M. Holt, and Gary K. Ackers, editors:
Methods in Enzymology, Vol. 455, Burlington: Academic Press, 2009, pp. 237-258.
ISBN: 978-0-12-374596-5

CHAPTER NINE

NMR Analysis of Dynein Light Chain Dimerization and Interactions with Diverse Ligands

Gregory Benison* *and* Elisar Barbar*,[1]

Contents

Abstract

NMR is a powerful tool for quantitative measurement of the thermodynamic properties of biological systems. In this review, we discuss the role NMR has played in understanding the various coupled equilibria in dimerization of dynein light chain LC8 and in its interactions with its ligands. LC8, a very highly conserved 89-residue homodimer also known as DYNLL, is an essential component of the dynein and Myosin V molecular motors and is also found in various other complexes. LC8 binds to disordered segments of its partners, promoting them to dimerize and form more ordered structures, often coiled coils. The monomer-dimer equilibrium is controlled by electrostatic interactions at the dimer interface, such as by phosphorylation of residue Ser88, which is a regulatory mechanism for LC8 *in vivo*. NMR experiments have uncovered several subtle interactions– weak dimerization of a phosphomimetic mutant, and allosteric interaction between the LC8 binding sites– that have been overlooked by other methods. NMR has also provided a residue-specific view of the titration of histidine residues at the LC8 dimer interface, and of a nascent helix in one of the binding partners, the primarily disordered dynein intermediate chain IC74. We give special attention to methods for quantitative interpretation of NMR spectra, an important consideration when using NMR to measure equilibria.

* Department of Biochemistry and Biophysics, Oregon State University, Corvallis, Oregon, USA
[1] Corresponding author: barbare@science.oregonstate.edu (541)-737-4143, (541)-737-0481 (fax)

Methods in Enzymology, Volume 455
ISSN 0076-6879, DOI: 10.1016/S0076-6879(08)04209-2

Dynein light chain LC8 is a highly conserved, essential component of the microtubule-based molecular motor dynein. As a dynein subunit, LC8 is involved in fundamental processes including retrograde vesicular trafficking, ciliary/flagellar motility and cell division. LC8 also interacts with non-dynein proteins in diverse systems, including some with roles in apoptosis, viral pathogenesis, enzyme regulation, and kidney development.

LC8 is a moderately tight homodimer (Barbar *et al.*, 2001, Liang *et al.*, 1999). Its interactions with a number of non-dynein proteins led to the widely held view that LC8 functions as a cargo adaptor. However, based on recent structural and thermodynamic studies we proposed that LC8 is not primarily a dynein subunit, but is an essential component of diverse protein complexes that play roles in a variety of cellular systems (Barbar, 2008). In its role in these diverse systems, LC8 fits the definition of a hub protein with a common mode of action. In dynein and in all other complexes, LC8 acts as a dimerization engine, promoting the dimerization and ordering of the natively disordered monomeric proteins with which it interacts (Benison *et al.*, 2006; Nyarko *et al.*, 2004; Wang *et al.*, 2004). Dimerization of LC8 is required for this activity because the monomer lacks the groove that is necessary for binding (Makokha *et al.*, 2004; Wang *et al.*, 2003). Interestingly, dimerization is disrupted by phosphorylation of a specific Ser residue at the interface, resulting in formation of an inactive monomer (Song *et al.*, 2007, 2008).

This review will focus on the use of NMR to understand four types of coupled equilibria: monomer-dimer equilibrium coupled to the electrostatic charge of a single interface residue, monomer-dimer equilibrium coupled to ligand binding, disorder to order transition in both LC8 and its binding partners coupled to ligand binding, and structural change in one subunit of the LC8 dimer coupled to ligand binding to the other subunit. These linkages were not apparent using other biochemical and biophysical techniques.

We will not address in this review NMR sample preparation or data collection. Rather, we will focus on NMR data analysis and in particular accurate measurement of peak intensities, a topic that has received less attention in the literature but is very important for thermodynamics measurements.

1. NMR Methodology

Exchanging populations. NMR is a useful tool for studying systems that exist in multiple interconvertible states. In proteins, these might be folded and unfolded conformations, or occupied and unoccupied binding sites. Remarkably, because of the minute energies involved in nuclear magnetic

transitions and their weak coupling with the rest of the system, NMR is capable of measuring populations and exchange rates in systems that remain unperturbed from thermodynamic equilibrium (Bain, 2003). The choice of NMR experiment and the type of conclusion that can be drawn depend on the relative populations of the different states and on the rate of exchange between them. Chemical exchange can be classified as fast, intermediate, or slow on the NMR time scale, and NMR can be used to study exchange processes in all of these regimes (Bain, 2008). When the exchange rate is significantly smaller than the chemical shift difference, the system is in slow exchange, and the NMR spectrum is simply the sum of the spectra of each population in the absence of exchange. The relative populations of the different states can be determined from the relative NMR signal intensities. Binding sites can be mapped by chemical shift perturbations. When the chemical shift difference and exchange rate are approximately equal, the system is in intermediate exchange, and the line widths become broader than what they would be without the exchange process. In practice the lines can become so broad that they are not observable above the noise level. With intermediate exchange, though populations cannot be as easily measured as in the case of slow exchange, it is still often possible to map binding sites to the residues that experience the most broadening. For systems in fast exchange the exchange rate is significantly larger than the chemical shift differences. The observed peak position is an average of its value in the various exchanging states weighted by the relative populations, and can therefore be used to measure the relative populations if the peak positions at the end points are known.

Even when only one state is significantly populated, conformational exchange with minor states can still be observed through its influence on NMR relaxation parameters (Palmer *et al.*, 2001). In particular, the exchange-derived contribution to transverse relaxation known as R_{ex} is useful for studying exchange processes in proteins on the μsec–msec time scale.

Data reduction. For thermodynamic studies by NMR, we need quantitative measurements of abstract peak parameters such as peak positions, intensities, and linewidths. These parameters are not measured directly; rather, they must be extracted from spectra which in their raw form are simply a collection of intensity measurements sampled regularly on a frequency grid (Fig. 9.1). We call the process of extracting useful parameters from raw spectra *data reduction*, a term borrowed from X-ray crystallography where it refers to the analogous process of converting raw diffraction images into collections of structure factors (Leslie, 2006). The simple and robust tools available for data reduction in crystallography have contributed to its success as a method in structural biology. In NMR, despite less emphasis on development of robust automated methods (Malmodin and Billeter, 2005), the data reduction process is just as critical.

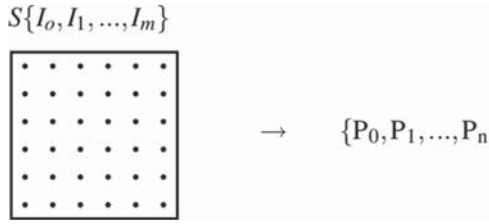

Figure 9.1 The data reduction problem. A spectrum (S) which is a set of *m* intensities $\{I_o \ldots\}$, usually sampled on a rectangular grid, is mapped to a set of *n* parameters $\{P_0 \ldots\}$. Parameters include peak intensities, positions, and linewidths. Which parameters are determined depends on the data reduction method used.

There are several methods available for extracting peak parameters from raw spectra and the choice of method depends on the application. For example, in collecting NOE restraints for structure determination by NMR, chemical shifts must be determined only well enough to allow assignment (Guntert, 1998). A typical tolerance for matching proton resonances is 0.02 ppm ($\sim 12Hz$ at a typical field strength); trying to achieve tighter tolerance may not result in improved assignments (Malmodin and Billeter, 2005). In contrast, meaningful measurement of residual dipolar couplings requires very accurate determination of peak positions: within 2 Hz or less (Bax *et al.*, 2001). In structure determination, intensities are often measured only accurately enough to place signals into coarse categories such as strong, medium, or weak. For the thermodynamic applications described in this review, it is desirable to measure populations (and therefore peak intensities) with the highest possible accuracy ($\sim$ 5% error is typical).

In our studies of dynein regulation and assembly we have used several data reduction strategies: ad-hoc analysis, integration, and modeling. An ad-hoc method relies on converting a spectrum to a visual representation such as a contour plot or a one-dimensional trace and then making an estimate of a parameter such as intensity or line width by looking at that visual representation. Ad-hoc methods can be very effective because they can leverage the ability of human visual processing to account subjectively for artifacts and overlap; however, this same subjectivity can introduce bias and is prone to over-interpreting the data, especially for weaker signals.

In integration, a subset of spectral intensities I_i are chosen and added to obtain a peak intensity parameter. An optimum integration box size can be chosen that makes the best compromise between including more points (to capture the most signal) and excluding points at the edge (to minimize the inclusion of noise) (Rischel, 1995). A smaller-than-optimum box may be chosen to minimize the problem of overlap. In the extreme case, the integration box can be shrunk to a single point (the local maximum of

the peak). This approach has the disadvantage of excluding some points that contain useful signal, and it does not solve completely the problem of overlap.

In modeling, the data reduction problem is performed in reverse: the peak parameters P_0 . . . are used to reconstruct the spectral intensities I_0, . . ., with some criterion such as the least-squared error being used to select the set of parameters that results in the best match between the reconstructed and the original spectrum. Modeling has been applied to NMR spectra both in the time domain (Andrec and Prestegard, 1998) and in the frequency domain (Denk *et al.*, 1986). Modeling is somewhat more complex than other data reduction methods but is the best strategy in cases of overlap, and also can take advantage of inherent relationships between signals to obtain better parameter estimates (Andrec and Prestegard, 1998). For example, a cross-peak and an auto-peak might rigorously share a common chemical shift and linewidth in one dimension; or, in an experiment involving decay as a function of mixing time, only the intensity may change as a function of mixing time and not the peak position. A reduction in the number of independent parameters is beneficial because there is generally a trade-off between the complexity of a model and how accurately its parameters can be determined. Often, information obtained from strong peaks can be used to help constrain the fitting of weaker but more interesting peaks. This also has an analogy in X-ray crystallography: low-resolution reflections are critical in determining the unit cell parameters, which are then used to constrain the measurement of the high-resolution reflections that provide the most information about the structure (Otwinowski and Minor, 1997).

All of the data reduction methods discussed above can be performed using the NMR visualization package burrow-owl (Benison *et al.*, 2007a), available from the authors or at http://burrow-owl.sourceforge.net. Given the minimal (by today's standards) computational resources needed, we recommend that full modeling be used whenever quantitative accuracy is important, making use of constraints from peak relationships where possible.

We will now review several insights about LC8 that have been gained through NMR, the role that chemical exchange has played, and the data reduction methods used.

2. Monomer-dimer Equilibrium Coupled to Electrostatics

LC8 is a symmetric dimer, with a β-sheet at the subunit interface composed of four strands from one subunit and one strand swapped over from the other subunit (Liang *et al.*, 1999). Dimerization is moderately

tight—K_d is 12 μM at 4 °C and neutral pH—and becomes weaker at low pH (Barbar *et al.*, 2001). The structure of the monomer in solution is quite similar to one chain of the dimer, except the swapped-over strand $\beta 3$ is a flexible loop rather than a structured β-strand (Makokha *et al.*, 2004; Wang *et al.*, 2003). The monomer-dimer equilibrium can be modulated by electrostatic interactions of two residues at the dimer interface: His55, which becomes protonated as a function of pH, and Ser88, which is a target for phosphorylation (Fig. 9.2). NMR has been important in elucidating the roles of both of these residues in controlling dimerization, as shown below.

Histidine pKa measurements. The wild-type dimer dissociates to a monomer at low pH, with a titration midpoint of pH 4.8 (Barbar *et al.*, 2001). This pH-induced dissociation is linked to titration of residue His55 (Nyarko *et al.*, 2005). When protonated, His55 inhibits dimerization by charge-charge repulsion with His55′. The histidine Hε and Cε chemical shifts, easily measured in ^{1}H-^{13}C HSQC spectra (Fig. 9.3A), are sensitive indicators of both protonation state of the histidine residue and monomer-dimer equilibrium. The dimerization reaction is slow on the NMR time scale, giving rise to separate peaks for the monomeric and dimeric forms. The monomer and dimer populations as a function of pH can be determined from the relative intensities of the corresponding peaks (Fig. 9.3B). In contrast, the protonation reaction is fast on the NMR time scale, giving rise to a single peak with a pH-dependent chemical shift. Titration curves for each histidine side chain individually can be measured by following the position of the Cε-Hε peak (Fig. 9.3c). These experiments demonstrate that systems often undergo multiple exchange processes on different time scales, and that NMR can be used to observe multiple exchange processes simultaneously. Uniquely amoung the three histidines of LC8, the protonation statue of His55 was identified as being coupled to dimerization because it has a pKa of 4.8, which corresponds to the macroscopic pKa determined from sedimentation equilibrium studies (Barbar *et al.*, 2001), and it shows

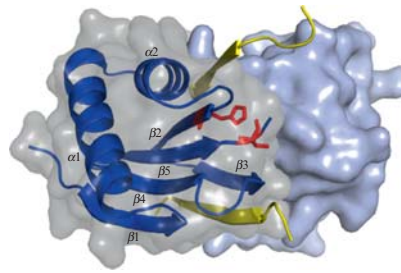

Figure 9.2 The symmetric dimer LC8. Residues Ser88 and His55, shown in red, influence the monomer-dimer equilibrium through electrostatic interactions at the dimer interface. Bound ligands are shown in yellow in the binding groove.

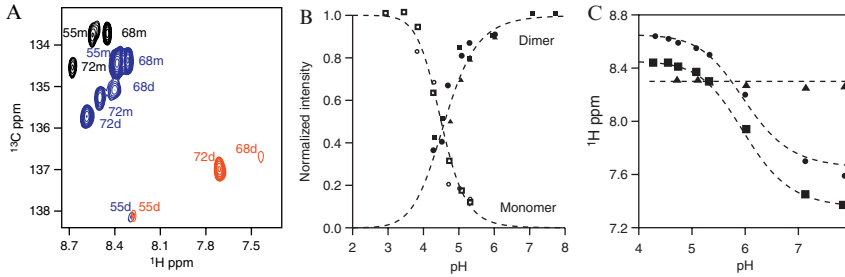

Figure 9.3 Titration of residue His55 is linked to dimerization [taken from (Nyarko *et al.*, 2005)]. (A) ^{1}H-^{13}C HSQC spectrum of wild-type LC8, showing Hε-Cε peaks for the three histidines, at pH 3 (black), pH 5 (blue), and pH 7 (red). 'd' and 'm' indicate peaks arising from dimer and monomer populations, respectively. (B) Monomer and dimer population as a function of pH, determined by following the peak intensities of the peaks in (A). (C) Titration curves for the histidines in the dimeric state, determined by following the proton chemical shifts of the peaks in (A).

no evidence of titrating in the dimeric state. The other two histidine residues (His68 and His72) exhibit typical pKa's of ~6.0 in the dimeric state. The mutant $LC8_{H55K}$-a nontitratable analogue for protonated His55-behaves as a monomer by size exclusion chromatography, and over a wide pH range has a spectrum resembling that of the pH-induced wild-type monomer (Nyarko *et al.*, 2005).

Measurement of dimer association and dissociation rates. Phosphorylation of LC8 is an important regulatory mechanism *in vivo*, as phosphorylation at Ser88 by Pak1 inhibits apoptosis and promotes cancerous phenotypes (Puthalakath *et al.*, 1999; Song *et al.*, 2008; Vadlamudi *et al.*, 2004). Dimerization is disrupted in the phosphomimetic mutant $LC8_{S88E}$ which elutes as a monomer on a gel-filtration column (Song *et al.*, 2007, 2008). ^{1}H-^{15}N HSQC spectra of $LC8_{S88E}$ collected at 1 m*M*, however, reveal the presence of a dimeric population (Fig. 9.4) in slow exchange with a monomeric population. From quantitation of peak intensities, the K_d for dimerization of $LC8_{S88E}$ is 1.4 m*M*, 100 times weaker than for wild type LC8 (Song *et al.*, 2007).

The association and dissociation rates for $LC8_{S88E}$ can be measured by monitoring exchange of N_Z magnetization (Farrow *et al.*, 1994). This is possible for systems where exchange is slow on the NMR time scale, yet not too slow that NMR signals decay before cross-peaks can build up ($k_{ex} \sim 0.5\ sec^{-1} - 5\ sec^{-1}$). $LC8_{S88E}$ falls into this favorable regime and crosspeaks are easily observed in N_Z exchange experiments (Fig. 9.5). In this experiment, magnetization is frequency-labeled with the ^{15}N chemical shift, transferred to the Z axis, then allowed to undergo chemical exchange for periods of up to ~500 msec.

The N_Z experiment is a good example of the benefits of spectral modeling as a means of extracting peak parameters (see earlier). The experiment is

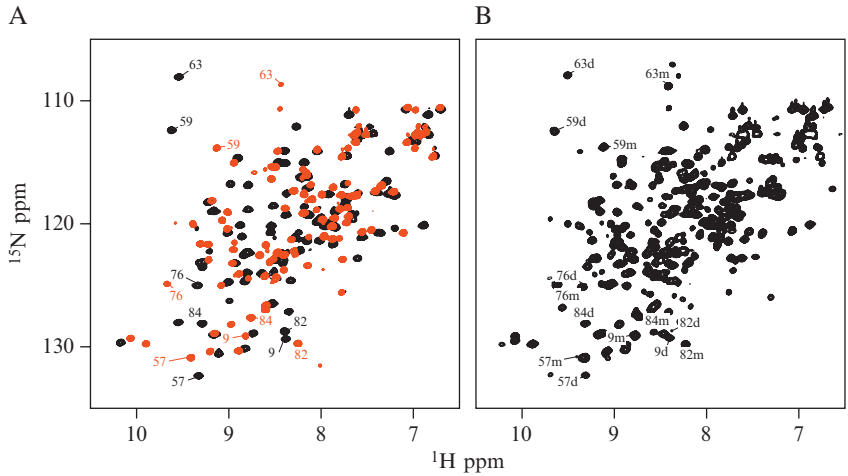

Figure 9.4 Monomeric and dimeric populations of $LC8_{S88E}$. (A) ^{1}H-^{15}N HSQC spectra of monomeric $LC8_{H55K}$ (red) overlayed on wild type LC8 (black). (B) HSQC spectrum of $LC8_{S88E}$ at 1 m*M*, which has the appearance of the superposition of the spectra in (A), showing that the sample contains a monomeric and a dimeric population in slow exchange. Taken from (Song *et al.*, 2007).

collected as a series of two-dimensional spectra taken at different mixing times. For each residue, each spectrum contains two crosspeaks and two autopeaks. Therefore, modeling a single residue in a typical experiment containing a series of six mixing times involves fitting $6 \times 4 \times (2 \times 2 + 1) = 120$ independent parameters if each peak is fit without considering its relationship to the others. The number of free parameters can be reduced to just 32 by recognizing that the peaks are related: for each residue, there is a ^{1}H chemical shift and linewidth for the monomeric and dimeric states, and an ^{15}N chemical shift and linewidth. These eight parameters (four chemical shifts, four linewidths) are sufficient to determine the positions of all the peaks in all the spectra, because the peak position does not change with mixing time and because the crosspeaks share positional parameters with the autopeaks. The intensity of each peak is still an independent function of mixing time. The total number of free parameters is therefore $8 + (6 \times 4) = 32$.

Association and dissociation rate constants k_{on} and k_{off} are determined by fitting the time course of the intensity of the cross- and auto-peaks. Magnetization evolves via a system of linear differential equations, and chemical exchange simply adds linear terms to this system (Bain, 2008). Because the system remains at thermodynamic equilibrium, the contribution of chemical exchange to the overall magnetization exchange rate remains constant. In the N_Z exchange experiment, two–site exchange of longitudinal magnetization between a monomeric environment (I_M) and a dimeric environment (I_M) is given by:

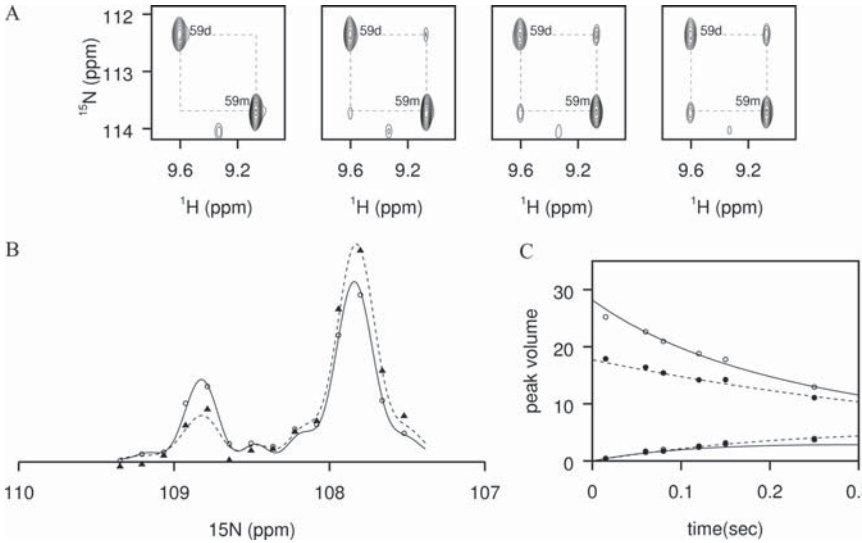

Figure 9.5 $LC8_{S88E}$ monomer-dimer exchange measured by N_Z-exchange spectra. (A) Excerpts around residues Asp37 and Gly59, respectively, from the longitudinal magnetization exchange experiment, with mixing times of (left to right) 15 msec, 80 msec, 150 msec, and 250 msec. Auto-peaks for the monomer and the dimer are labeled m and d, respectively. (B) One-dimensional profile through an auto-peak (right) and a cross-peak (left) at 150 msec mixing time (circles, solid line) and 60 msec mixing time (triangles, dashed line). Solid lines correspond to the model described in the text from which the peak parameters are taken. (C) Peak intensities as a function of mixing time. The dimer-dimer autopeak and dimer-monomer crosspeak intensities are shown with dashed lines and solid symbols. The monomer-monomer autopeak and monomer-dimer crosspeak intensities are shown with solid lines and open symbols. The lines are fits to a monomer-dimer chemical exchange model.

$$\begin{aligned}[\dot{I}_M] &= -k_-[I_M] + k_-[I_D] - R_M[I_M] \\ [\dot{I}_D] &= k_+[I_M] - k_-[I_D] - R_D[I_D]\end{aligned} \tag{9.1}$$

where R_M and R_D are the longitudinal relaxation rates for monomer and dimer, respectively. For this bimolecular reaction, the magnetization exchange rate constants k_+ and k_- must be distinguished from the chemical exchange rate constants k_{on} and k_{off} of the $LC8_{S88E}$ dimerization reaction:

$$2M \underset{k_{off}}{\overset{k_{on}}{\rightleftharpoons}} D$$

The magnetic and chemical rate constants are related by the equations $k_+ = k_{on}M$ and $k_- = k_{off}$. The monomer concentration M is a constant and can be calculated from the (known) total protein concentration and the rate constants k_{on} and k_{off}; therefore k_{on} and k_{off} are sufficient to determine k_+

and k_. Because temperature can be controlled precisely in the NMR experiment, the dependence of k_{on} and k_{off} on temperature can be measured, which in turn allows determination of ΔH^0, ΔS^0, and the activation energy for dimerization (Benison *et al.*, 2009, in preparation).

3. Dimerization is Coupled to Ligand Binding

The ligand-binding groove of LC8 is at the interface of the two subunits, and the bound ligand makes contacts with both subunits (Benison *et al.*, 2007b; Liang *et al.*, 1999). The swapped-over β-strand, which forms part of the binding site, becomes less ordered in the monomer (Makokha *et al.*, 2004). These observations suggest that only the dimer has ligand-binding ability. Hence, the mutant $LC8_{H55K}$, which is entirely monomeric, has no ligand-binding ability (Fig. 9.6).

Surprisingly, the mutant $LC8_{S88E}$, which is primarily monomeric, retains considerable binding capability in a GST pulldown assay (Fig. 9.6). In a fluorescence assay of 50 μM $LC8_{S88E}$ and 1 μM of the ligand Bim, where the $LC8_{S88E}$ is mostly monomeric, less than 10% of the ligand is bound (Song *et al.*, 2008), confirming that the ligand cannot bind the monomeric form. However, at higher concentrations of $LC8_{S88E}$ in NMR experiments, a population with a spectrum resembling that of the wild-type complex appears as the ligands IC and Swa are titrated in (Fig. 9.7)—the ligands bind to the dimeric form and eventually shift the equilibrium entirely to dimer (Song *et al.*, 2007). Since the monomeric, dimeric, and ligated forms are all in slow exchange, their populations as a function of ligand concentration can be measured from the peak intensities.

Figure 9.6 GST pulldown assays showing interaction of $IC^{92–237}$ fused to GST with LC8 WT and mutants. The presence of a low-molecular-weight band indicates binding, and the intensity of the band indicates the efficiency of binding. (lane 1): Purified GST-$IC^{92–237}$ in the absence of any lysates; (lane 2): with wild-type LC8 as a positive control; (lane 3): with monomeric $LC8_{H55K}$, showing no binding; (lane 4): with $LC8_{S88E}$, showing partial binding.

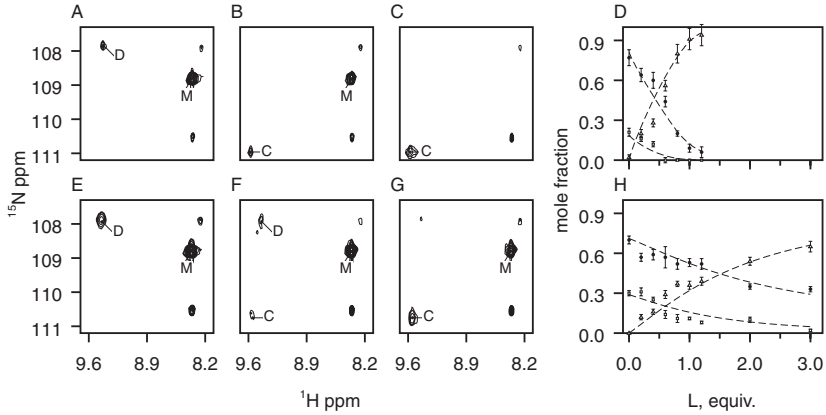

Figure 9.7 Binding of ligands promotes the dimerization of $LC8_{S88E}$. (A-D), (E-H) Titration with short peptides corresponding to the LC8-binding sites of the proteins Swallow (Swa) and IC74, respectively. Excerpts of ^{1}H-^{15}N HSQC spectra containing residue Gly63 at 0 equivalents (A, E), 0.4 equivalents (B, F), and 1.0 equivalents (C, G) show populations of monomeric LC8 (M), dimeric LC8 (D), and the LC8/peptide complex (C) in slow exchange. (D, H) Mole fractions of monomer (circle), dimer (square), and complex (triangle) as a function of ligand equivalents. Curves were calculated from the law of mass action using the K_d for $LC8_{S88E}$ association and a K_d for ligand binding. More tightly-bound ligands such as Swa are more efficient in shifting the monomer-dimer equilibrium towards the dimer. Reproduced from (Song *et al.*, 2007).

Affinities for dimerization and ligand binding can be determined by fitting the intensities to theoretical titration curves derived from mass-action laws:

$$2\,(\mathrm{LC8}) \underset{}{\overset{K}{\rightleftharpoons}} (\mathrm{LC8})_2 \overset{2X,\ K_1}{\rightleftharpoons} (\mathrm{LC8})_2\mathrm{X}_2$$

Where X is the ligand, $K = [(LC8)_2]/[(LC8)]$ is the monomer-dimer equilibrium constant and $K_1 = [X][(LC8)_2]/[(LC8)_2X] = [X][(LC8)_2X]/[(LC8)_2X_2]$ is the ligand dissociation constant. Despite the high similarity of the structures of LC8/Swa and LC8/IC (Benison *et al.*, 2007b), Swa binds $LC8_{S88E}$ with 100-fold greater affinity than IC. Note that in the preceding analysis a single dissociation constant is used to describe the first and second ligand-binding steps. A more complicated model, in which these are allowed to be different, is not justified by the $LC8_{S88E}$ titration data, but other experiments (described below) can detect small differences in the dissociation constants of the first and second binding steps.

4. Folding is Coupled to Binding

The N-terminal segment of dynein intermediate chain IC74 is an excellent example of a natively disordered protein that forms a partially folded structure as part of a larger complex. A significant number of such

proteins are now recognized, many of them having regulatory functions (Dyson and Wright, 2005b). The role of LC8 as a folding scaffold for IC74 has been described using a variety of techniques including limited proteolysis, circular dichroism spectroscopy, fluorescence, and NMR (Benison *et al.*, 2006; Makokha *et al.*, 2002; Nyarko *et al.*, 2004). NMR has been useful both in mapping the direct interaction of LC8 and IC74 and in describing induced folding in IC74 distant from the binding site. Similar phenomena have been recognized or predicted in other LC8 binding partners (Barbar, 2008; Wang *et al.*, 2004).

Mapping the binding site in IC74. The N-terminal segment of the dynein intermediate chain IC74 is variable and subject to alternative splicing, yet contains a highly conserved "TQT box" (Nurminsky *et al.*, 1998). This TQT box is protected from limited proteolysis by the binding of LC8 (Makokha *et al.*, 2002). In a series of IC74 deletion mutants, only those containing the TQT box had LC8 binding affinity, and a small peptide corresponding to the TQT box region bound to LC8 (Lo *et al.*, 2001). With NMR, all the specific residues in IC74 perturbed upon binding can be assigned. The construct $IC74^{84–143}$ contains the LC8 binding site and some flanking residues. When a ^{15}N-labeled segment of $IC74^{84–143}$ is mixed with an unlabeled sample of LC8, certain signals of $IC74^{84–143}$ vanish (Fig. 9.8) due to an intermediate exchange process between free and complexed $IC74^{84–143}$ or between ordered and disordered conformations (Benison *et al.*, 2006). The most-broadened peaks correspond to residues with the largest change in chemical environment upon binding LC8. The remaining residues show no change in chemical shift, which demonstrates that their conformation does not change appreciably upon binding: in a 60-residue segment around the LC8 binding site, IC74 remains disordered outside the small recognition motif (residues 126–134).

Nascent order in a distal site. Although the segment immediately adjacent to the binding site does not gain secondary structure upon forming the complex, circular dichroism shows that binding of LC8 causes a modest increase in the helical content of the N-terminal segment of IC74, indicating the formation of a ~24-residue helix. There are two predicted coiled-coil domains in the disordered N-terminal domain of IC74: one C-terminal to the LC8 binding site (residues 210–240) and one N-terminal (residues 1-30). In CD spectra of smaller domains containing the LC8 binding site and just one of these predicted coiled coils, the construct $IC74^{1–143}$ showed little change upon binding LC8, but the segment $IC74^{114–260}$ showed increased helical content similar to that seen for the full N-terminal domain (Nyarko *et al.*, 2004). The residues in the predicted coiled-coil around residue 230 are also protected from proteolysis by binding of LC8, despite being 100 residues distant from the LC8 binding site. Though this domain containing the predicted coiled coil is

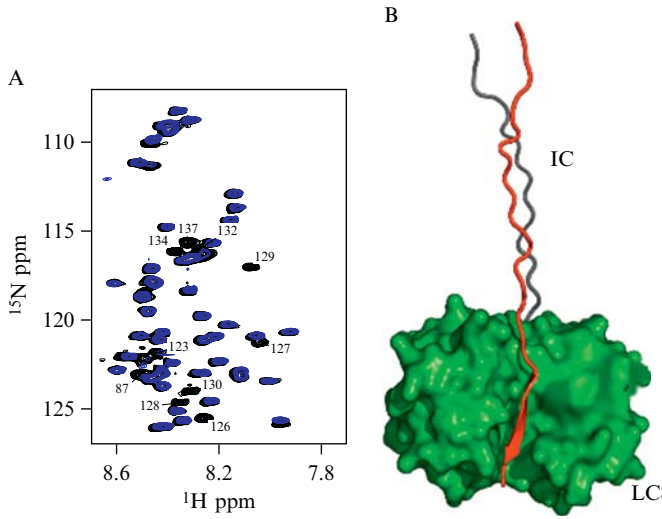

Figure 9.8 Binding of LC8 to IC74$^{84–143}$. (A) Overlay of ^{1}H-^{15}N HSQC spectra of ^{15}N-labeled IC74$^{84–143}$ (black) and a 1:1 mixture of IC74$^{84–143}$ with unlabeled LC8 (blue). All peaks arise from IC74$^{84–143}$, because LC8 is not isotopically labeled. Labeled peaks correspond to those that are more than 80% attenuated in the complex. Taken from (Benison *et al.*, 2006). (B) A model of the LC8 dimer bound to two chains of IC74. Residues in the binding site undergo intermediate conformational exchange, leading to peak broadening. Residues adjacent to the binding site remain disordered.

disordered completely in the absence of LC8, it has some intrinsic propensity to fold into a helix: addition of the osmolyte TMAO induces an increase in helicity that somewhat mimics what is observed upon binding of LC8. NMR spectroscopy provides a per-residue picture of this induced folding process. In unfolded proteins, the observation of sequential NOE signals often indicates the presence of latent secondary structure (Dyson and Wright, 2005a). In the construct IC74$^{198–237}$, which contains the predicted coiled-coil but not the LC8 binding site, the presence of sequential HN-HN NOE's clearly indicates a nascent helix (Fig. 9.9). Thus, even though this segment appears completely unfolded by CD, there is clear evidence for its propensity to form a coiled coil (Benison *et al.*, 2006).

Induced folding in LC8. LC8 is a well-ordered protein, leading to the view that it is a stable scaffold for the folding of disordered partners such as the dynein intermediate chain. However, the reverse is also true: LC8 itself is only fully folded when bound to one of its ligands. Apo-LC8 exhibits a small degree of flexibility that decreases upon forming a complex. Because the degree of

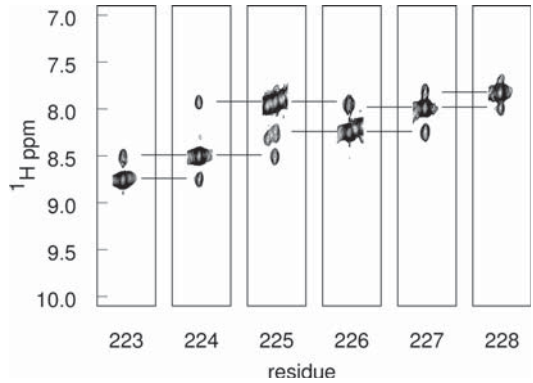

Figure 9.9 Evidence for a nascent helix in IC74. Strip plots from 3D ^{1}H-^{15}N NOESY-HSQC experiments recorded on ^{15}N-labeled IC74$^{198–237}$ showing sequential amide-amide NOE connectivities indicated by horizontal lines. A complete set of strong amide-amide NOE's for residues 223–228 at 5 °C is typical of the 2.6–2.8 Å distances in α-helices. Taken from (Benison *et al.*, 2006).

flexibility in free LC8 is so much smaller than in the free ligands, it cannot be detected by methods like CD that report only on the overall ordered structure but it has been well-described by NMR experiments which can focus on the disordered regions and measure disorder on different time scales.

The disorder in apo-LC8 is reflected by backbone ^{15}N relaxation, which is a sensitive indicator of disorder and dynamics. In particular, the relaxation rates of apo-LC8 cannot be accounted for by the tumbling of a single rigid conformation; it is necessary to include R_{ex} terms indicating conformational exchange on the ms-μs time scale (Fan *et al.*, 2002; Hall *et al.*, 2008). The R_{ex} terms are not distributed evenly over the sequence, but localized to the binding groove indicating that these are the residues most affected by the conformational exchange. Upon forming a complex with a peptide derived from the KXTQT ligand Bim, nearly all of the conformational exchange vanishes — the complex behaves nearly like a rigid, single conformation. A similar result is observed for LC8/Swa (Hall *et al.*, 2008). The disappearance of R_{ex} terms demonstrates that binding incurs an entropic cost due to changes in the protein itself in addition to those arising from the solvent and ligand.

The increased order of LC8 complexes relative to apo-LC8 is also reflected in better protection from amide proton exchange with the solvent, measured by NMR as H/D exchange (Benison *et al.*, 2007b; Fan *et al.*, 2002). Amide exchange rates are (as expected) reduced in the β-strand that directly contacts the ligand, but are also reduced in the interior β-strands, with the effect decreasing with increasing distance from the ligand-binding site. Thus ligand binding appears to reduce flexibility of the entire β-sheet.

The conserved glutamine residue of the ligand also forms a cap for the N-terminal of LC8 helix α2, and the amide exchange rates of the first few residues of this helix are greatly reduced in the complex.

Interestingly, ^{15}N relaxation demonstrates some disorder-to-order transition upon the monomer-to-dimer transition as well. There are residues distant from the dimer interface which display R_{ex} behavior in the constitutively monomeric mutant $LC8_{H55K}$, but not in the wild-type dimer (Hall *et al.*, 2008). Thus LC8 exists in three states, ranging from least to most ordered: monomeric, dimeric, and complexed; with the monomeric form mostly ordered but with extensive heterogeneous dynamics, and the complexed form behaving almost as a rigid body.

5. Allostery in LC8

NMR evidence for allosteric interaction. LC8 has two identical ligand-binding sites at the dimer interface, which raises the interesting possibility of allosteric interaction (Fig. 9.10A). Crystal structures of free LC8 and several of its complexes have revealed a possible mechanism for such allostery: ligand binding is associated with an expansion of the peptide-binding groove due to shear motion at the dimer interface (Benison *et al.*, 2008). Since this is primarily a change in the quaternary structure, binding of the first ligand could cause a global conformational shift that pre-organizes the second ligand binding site (Fig. 9.10B). Many oligomeric proteins which can undergo a shift in quaternary structure exhibit this type of allostery (Changeux and Edelstein, 2005). Crystallography has therefore defined a possible mechanism for allostery but has not provided any direct evidence for it, because there are no crystal structures of singly bound intermediates. Through NMR, however, it has been possible to characterize singly bound intermediates in solution.

Titration monitored by NMR can provide evidence for allosteric interactions, because the number of unique conformational environments is reflected in the number of distinct chemical shifts that can be observed for each atom (Stevens *et al.*, 2001). Theoretically, four distinct environments are possible for each residue: one for the free state, one for the doubly bound state, and two for the singly bound state (which lacks symmetry). However, in practice, for most residues less than four peaks are observed due to chemical shift degeneracy. If it is assumed that there is no allosteric interaction (i.e., binding at one site is accompanied by small local conformational changes, but no global changes that affect the conformation at the other site), each atom is expected to have only two possible chemical shifts because the two conformational environments in the singly bound state are degenerate with those of the free and doubly bound states. If binding of

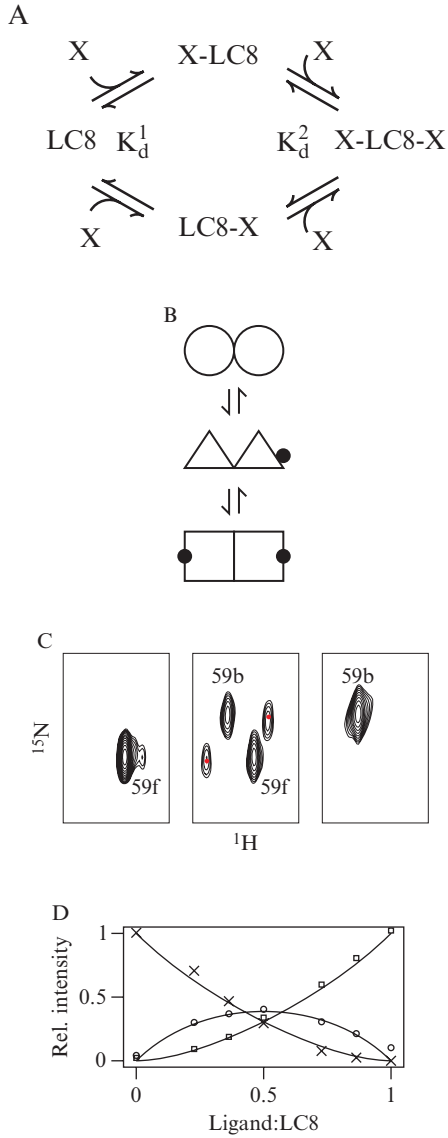

Figure 9.10 Model and evidence for allostery in LC8. (A) The two binding steps of LC8. X is the ligand. The two dissociation constants are defined as $K_d^1 = [LC8][X]/[LC8 - X]; K_d^2 = [LC8 - X][X]/[X - LC8 - X]$. The binding sites and ligands are identical, so [LC8-X] = [X-LC8]. (B) A model for allostery in LC8 binding. Different polygonal shapes represent different conformations of LC8 and a black dot indicates an occupied ligand-binding site. (C) NMR evidence for allostery. Excerpts of of ^{1}H-^{15}N HSQC spectra of ^{15}N-labeled LC8 titrated with unlabeled nNOS peptide at

the first ligand is associated with a global conformational change (as in Fig 9.10B), it is expected that for some residues this degeneracy will be removed, giving rise to intermediate peaks during titration. Such intermediate peaks are observed during titration of ^{15}N-labeled LC8 with unlabeled ligands (Fig. 9.10C), confirming that there is allosteric interaction.

An intriguing consequence of allosteric interaction between the binding sites is that the first and second binding constants K_d^1 and K_d^2 can be different. The ratio K_d^1/K_d^2 is sufficient for calculating a theoretical titration curve by solving the following system of equations:

$$\begin{gathered} \frac{[\mathrm{LC8}] \times [\mathrm{X-LC8-X}]}{[\mathrm{X-LC8}] \times [\mathrm{LC8-X}]} = \frac{K_d^1}{K_d^2} \\ [\mathrm{X-LC8}] = [\mathrm{LC8-X}] \\ [\mathrm{LC8}] + [\mathrm{X-LC8}] + [\mathrm{LC8-X}] + [\mathrm{X-LC8-X}] = 1 \end{gathered} \tag{9.2}$$

For titration with the ligand nNOS (Fig. 9.10D), $K_d^1/K_d^2 = 2.5$ is the smallest (i.e., most conservative) ratio that provides a good fit to the data. The modest increase in binding affinity for the second binding event is consistent with an additional expansion of the binding groove accompanying the second ligation.

NMR Data Reduction. The NMR titration experiments pose a challenge for NMR data reduction for several reasons. First, the most useful information (the population of the singly bound form) is carried by weaker signals (the intermediate peaks) in the presence of stronger signals (the apo and bound peaks); to be accurate, the weak signals must be measured with minimum interference from the strong ones. Second, peak overlap is an issue: although LC8 contains only a moderate number of residues (89), the HSQC spectrum becomes crowded during titration due to the presence of up to four peaks per residue. Thus for LC8/nNOS, only one residue (Gly59) shows four peaks entirely well-separated from each other and from all other signals (Fig. 9.10C). For all other residues with all ligands tested, the intermediate peaks suffer some degree of overlap. For this reason, modeling is the most useful data reduction method. A typical case is shown in (Fig. 9.11) for residue 37 during titration with nNOS; it is clear that full modeling is necessary to obtain reliable estimates of intensity.

(left to right) 0, 0.4, and 1.0 equivalents. Peaks for free LC8 (apo) and bound LC8 (doubly-occupied) are labeled 'f' and 'b', respectively. In the middle of the titration curve (middle panel), new peaks appear, which arise from singly bound LC8. (D) Titration curve for the resonances shown in (C). Crosses: free peak; circles: sum of intermediate peaks; squares: bound peaks. Curves represent populations predicted by the two-site binding model or $K_d^1/K_d^2 = 2.5$.

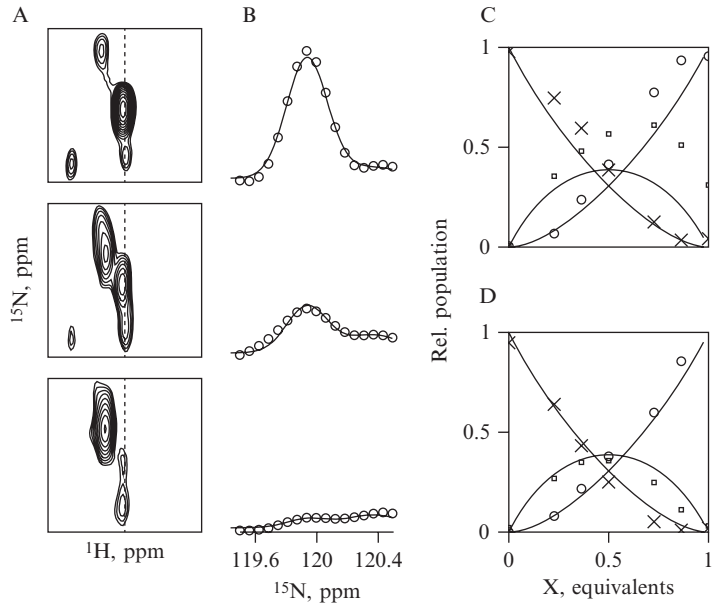

Figure 9.11 Reduction of NMR titration data. (A) Small excepts of HSQC spectra (centered around the peak from residue 37) taken during the titration of ^{15}N-labeled LC8 with a peptide derived from the ligand nNOS. Top to bottom: 0.2, 0.4, and 0.8 equivalents of ligand. (B) 1D slices along the ^{15}N dimension, indicated by the dashed lines in (A). Dots represent the experimental data and the solid lines represent the models used for profile fitting, which are the sum of two 2D gaussian lineshapes, one for the apo-peak and one for the intermediate peak (which can be seen immediately downfield from the apo peak). (C) Integrated intensities for the apo (crosses), intermediate (squares), and bound (circles) peaks. Due to overlap, the measured relative populations add up to a total greater than 1.0, and the agreement with the theoretical titration curve is poor. (D) Intensities derived from profile fitting to a sum of 2D gaussians. The theoretical titration curves correspond to a K_d^1/K_d^2 ratio of 2.5, and agree well with curves from other residues with better-resolved peaks.

In the titration experiment, like in the N_Z exchange experiment described above, it is useful to exploit relationships between peaks to reduce the number of free parameters to be determined during modeling. Treating each peak independently, for each residue there are $4 \times 5 \times n$ independent parameters (where n is the number of titration points). However, if the system behaves in the limit of slow exchange, then peak position and linewidth do not change throughout the titration, so that the number of independent parameters is $4 \times (4 + n)$. Thus for a typical titration of 8 data points, the number of free parameters can be reduced from 160 to 48. This is an example of the well-known tradeoff between the complexity of a model and how accurately its parameters can be determined: assuming constant peak positions and widths allows more accurate determination of

minor populations, because the positions of weak peaks are constrained by the corresponding peaks at other points along the titration curve where the population is higher. Alternately, treating the peaks independently allows for the possibility that the system does not behave strictly as a system in slow exchange (i.e., peak position and linewidth can vary with titration). In the case of LC8 titrations, we find the simpler model the more appropriate tradeoff given the degree of overlap in the spectra.

6. Summary

Our understanding of the role of LC8 in the assembly of dynein and other complexes has improved greatly in recent years, and much of this understanding has come from NMR. Contributions from NMR have been important in elucidating: the role of electrostatics at the dimer interface in LC8 monomer-dimer equilibrium; the coupling of ligand binding and dimerization; the coupling of folding and binding in LC8 and its partners; and allostery in LC8 binding.

NMR has several unique advantages as a tool for studying protein complex assembly. Often, NMR is complementary to other methods: for example, a nascent helix in IC74 was predicted from sequence analysis and CD spectroscopy, and then observed by NMR. Crystallography suggested a mechanism for allostery in LC8 binding, and NMR provided evidence for it. More importantly, NMR can be used to observe processes that are difficult to observe by other methods, either because they involve only small changes in energy (such as the weak dimerization of $LC8_{S88E}$) or because they involve only minor populations (such as the residual disorder in apo-LC8 or the nascent order in IC74). NMR can provide a per-residue view of a process understood in coarser detail by other methods: for example, sedimentation analysis suggested a connection between LC8 dimerization and titration of a histidine residue, and NMR identified His55 as the single histidine of the three in LC8 to behave this way. Sequence comparison and limited proteolysis roughly mapped a binding site for LC8 on IC74, and NMR then delineated the binding site precisely.

Several specific strategies have contributed to the success of NMR as a tool for studying assembly in the dynein complex. Despite advances in NMR analysis of large systems, it is still desirable to work with the smallest system possible. Small constructs often retain the essential features of the larger system from which they are derived— in IC74, a successful strategy was to study the binding domain and the nascent helix domain individually. Differential labeling has been useful for simplifying the analysis of complexes: many of the experiments described in this review involve forming a complex where only one component is labeled with NMR-active nuclei.

Finally, careful attention to data reduction techniques is crucial when studying exchanging populations where weak signals are often the most interesting. Modeling is the most general technique and the best for leveraging the natural relationships between NMR signals. Even complicated spectra can be modeled quite quickly by modern computers, so we find it worthwhile in most quantitative NMR studies.

In conclusion, NMR can be the key to a more rigorous, residue-specific, thermodynamic characterization of a biomolecular system, possibly uncovering phenomena such as weak associations or allosteric interactions that have been missed by other methods.

REFERENCES

Andrec, M., and Prestegard, J. (1998). A Metropolis monte carlo implementation of Bayesian time-domain parameter estimation: Application to coupling constant estimation from antiphase multiplets. *J. Magn. Reson.* **130,** 217–232.

Bain, A. (2003). Chemical exchange in NMR. *Prog. Nucl. Magn. Reson. Spectrosc.* **43,** 63–103.

Bain, A. (2008). Chemical exchange. *Annual Reports on NMR spectroscopy,* **63,** 23–48.

Barbar, E. (2008). Dynein light chain LC8 is a dimerization hub essential in diverse protein networks. *Biochemistry* **47,** 503–508.

Barbar, E., Kleinman, B., Imhoff, D., Li, M., Hays, T., and Hare, M. (2001). Dimerization and folding of LC8, a highly conserved light chain of cytoplasmic dynein. *Biochemistry* **40,** 1596–1605.

Bax, A., Kontaxis, G., and Tjandra, N. (2001). Dipolar couplings in macromolecular structure determination. *Methods Enzymol.* **339,** 127–174.

Benison, G., Berkholz, D., and Barbar, E. (2007a). Protein assignments without peak lists using higher-order spectra. *J. Magn. Reson.* **189,** 173–181.

Benison, G., Karplus, P., and Barbar, E. (2007b). Structure and dynamics of LC8 complexes with KXTQT-motif peptides: Swallow and dynein intermediate chain compete for a common site. *J. Mol. Biol.* **371,** 457–468.

Benison, G., Nyarko, A., and Barbar, E. (2006). Heteronuclear NMR identifies a nascent helix in intrinsically disordered dynein intermediate chain: Implications for folding and dimerization. *J. Mol. Biol.* **362,** 1082–1093.

Benison, G., Karplus, P. A., and Barbar, E. (2008). The Interplay of Quaternary Structure and Ligand Binding in the Diverse Interactions of Dynein Light Chain LC8. *J. Mol. Biol.* **384,** 954–966.

Changeux, J., and Edelstein, S. (2005). Allosteric mechanisms of signal transduction. *Science* **308,** 1424–1428.

Denk, W., Baumann, R., and Wagner, G. (1986). Quantitative evaluation of cross peak intensities by projection of two-dimensional NOE spectra on a linear space spanned by a set of reference resonance lines. *J. Magn. Reson.* **67,** 386–390.

Dyson, H., and Wright, P. (2005a). Elucidation of the protein folding landscape by NMR. *Methods Enzymol.* **394,** 299–321.

Dyson, H., and Wright, P. (2005b). Intrinsically unstructured proteins and their functions. *Nat. Rev. Mol. Cell Biol.* **6,** 197–208.

Fan, J., Zhang, Q., Tochio, H., and Zhang, M. (2002). Backbone dynamics of the 8 kDa dynein light chain dimer reveals molecular basis of the protein's functional diversity. *J. Biomol. NMR* **23,** 103–114.

Farrow, N. A., Zhang, O. W., Forman-Kay, J. D., and Kay, L. E. (1994). A heteronuclear correlation experiment for simultaneous determination of ^{15}N longitudinal decay and chemical-exchange rates of systems in slow equilibrium. *J. Biomol. NMR* **4,** 727–734.

Guntert, P. (1998). Structure calculation of biological macromolecules from NMR data. *Q. Rev. Biophys.* **31,** 145–237.

Hall, J., Hall, A., Pursifull, N., and Barbar, E. (2008). Differences in dynamic structure of LC8 monomer, dimer, and dimer-peptide complexes. *Biochemistry* **47,** 11940–11952.

Leslie, A. (2006). The integration of macromolecular diffraction data. *Acta Crystallogr D. Biol. Crystallogr.* **62,** 48–57.

Liang, J., Jaffrey, S., Guo, W., Snyder, S., and Clardy, J. (1999). Structure of the PIN/LC8 dimer with a bound peptide. *Nat. Struct. Biol.* **6,** 735–740.

Lo, K., Naisbitt, S., Fan, J., Sheng, M., and Zhang, M. (2001). The 8-kDa dynein light chain binds to its targets via a conserved (K/R)XTQT motif. *J. Biol. Chem.* **276,** 14059–14066.

Makokha, M., Hare, M., Li, M., Hays, T., and Barbar, E. (2002). Interactions of cytoplasmic dynein light chains Tctex-1 and LC8 with the intermediate chain IC74. *Biochemistry* **41,** 4302–4311.

Makokha, M., Huang, Y., Montelione, G., Edison, A., and Barbar, E. (2004). The solution structure of the pH-induced monomer of dynein light-chain LC8 from *Drosophila*. *Protein Sci.* **13,** 727–734.

Malmodin, D., and Billeter, M. (2005). High-throughput analysis of protein NMR spectra. *Prog. Nucl. Magn. Reson. Spectrosc.* **46,** 109–129.

Nurminsky, D., Nurminskaya, M., Benevolenskaya, E., Shevelyov, Y., Hartl, D., and Gvozdev, V. (1998). Cytoplasmic dynein intermediate-chain isoforms with different targeting properties created by tissue-specific alternative splicing. *Mol. Cell Biol.* **18,** 6816–6825.

Nyarko, A., Cochrun, L., Norwood, S., Pursifull, N., Voth, A., and Barbar, E. (2005). Ionization of His 55 at the dimer interface of dynein light-chain LC8 is coupled to dimer dissociation. *Biochemistry* **44,** 14248–14255.

Nyarko, A., Hare, M., Hays, T., and Barbar, E. (2004). The intermediate chain of cytoplasmic dynein is partially disordered and gains structure upon binding to light-chain LC8. *Biochemistry* **43,** 15595–15603.

Otwinowski, Z., and Minor, W. (1997). Processing of X-ray diffraction data collected in oscillation mode. *Methods in Enzymology* **276,** 307–326.

Palmer, A., Kroenke, C., and Loria, J. (2001). Nuclear magnetic resonance methods for quantifying microsecond-to-millisecond motions in biological macromolecules. *Methods Enzymol.* **339,** 204–238.

Puthalakath, H., Huang, D., O'Reilly, L., King, S., and Strasser, A. (1999). The proapoptotic activity of the Bcl-2 family member Bim is regulated by interaction with the dynein motor complex. *Mol. Cell* **3,** 287–296.

Rischel, C. (1995). Fundamentals of peak integration. *J. Magn. Reson. A* **116,** 255–258.

Song, C., Wen, W., Rayala, S., Chen, M., Ma, J., Zhang, M., and Kumar, R. (2008). Serine 88 phosphorylation of the 8-kDa dynein light chain 1 is a molecular switch for its dimerization status and functions. *J. Biol. Chem.* **283,** 4004–4013.

Song, Y., Benison, G., Nyarko, A., Hays, T., and Barbar, E. (2007). Potential role for phosphorylation in differential regulation of the assembly of dynein light chains. *J. Biol. Chem.* **282,** 17272–17279.

Stevens, S., Sanker, S., Kent, C., and Zuiderweg, E. (2001). Delineation of the allosteric mechanism of a cytidylyltransferase exhibiting negative cooperativity. *Nat. Struct. Biol.* **8,** 947–952.

Vadlamudi, R., Bagheri-Yarmand, R., Yang, Z., Balasenthil, S., Nguyen, D., Sahin, A., den Hollander, P., and Kumar, R. (2004). Dynein light chain 1, a p21-activated kinase 1-interacting substrate, promotes cancerous pheno-types. *Cancer Cell* **5,** 575–585.

Wang, L., Hare, M., Hays, T., and Barbar, E. (2004). Dynein light chain LC8 promotes assembly of the coiled-coil domain of swallow protein. *Biochemistry* **43,** 4611–4620.

Wang, W., Lo, K., Kan, H., Fan, J., and Zhang, M. (2003). Structure of the monomeric 8-kDa dynein light chain and mechanism of the domain-swapped dimer assembly. *J. Biol. Chem.* **278,** 41491–41499.